Measurement and Modeling of Air-Broadened Methane Absorption in the MERLIN Spectral Region at Low Temperatures

T. Delahaye, M. Ghysels, T. Hodges, K. Sung, Raymond Armante, H. Tran

JGR Atmospheres

RESEARCH ARTICLE
10.1029/2018JD028917

Measurement and Modeling of Air-Broadened Methane Absorption in the MERLIN Spectral Region at Low Temperatures

T. Delahaye[1], M. Ghysels[2], J. T. Hodges[2], K. Sung[3], R. Armante[1], and H. Tran[4]

[1]Laboratoire de Météorologie Dynamique, IPSL, CNRS, Ecole polytechnique, Université Paris-Saclay, Palaiseau, France, [2]National Institute of Standards and Technology, Gaithersburg, MD, USA, [3]Jet Propulsion Laboratory, California Institute of Technology, Pasadena, CA, USA, [4]Laboratoire de Météorologie Dynamique, IPSL, CNRS, Sorbonne Université, École normale supérieure, PSL Research University, École polytechnique, Paris, France

Key Points:
- Absorption cross sections of methane in the MERLIN spectral region is accurately measured and modeled for various *P* and *T* conditions
- Our model is capable to represent measured absorption to within 0.1% at the MERLIN online position
- Comparison with atmospheric measurement shows significant improvement with respect to existing spectroscopic modeling of CH_4 absorption

Correspondence to:
H. Tran,
ha.tran@lmd.jussieu.fr

Citation:
Delahaye, T., Ghysels, M., Hodges, J. T., Sung, K., Armante, R., & Tran, H. (2019). Measurement and modeling of air-broadened methane absorption in the MERLIN spectral region at low temperatures. *Journal of Geophysical Research: Atmospheres*, *124*, 3556–3564. https://doi.org/10.1029/2018JD028917

Received 29 APR 2018
Accepted 18 FEB 2019
Accepted article online 25 FEB 2019
Published online 20 MAR 2019

Abstract The ability to precisely model methane absorption in the R(6) manifold of the $2\nu_3$ band at atmospheric pressure and temperature conditions is a key technical requirement of the German-French, Methane Remote Sensing Lidar (MERLIN) space mission. To this end, 27 high-resolution and high-signal-to-noise-ratio absorption spectra of air-broadened $^{12}CH_4$ were recorded using a variable-temperature frequency-stabilized cavity ring-down spectroscopy apparatus. The measurement conditions corresponded to sample temperature, pressure, and methane molar fraction values spanning 220–290 K, 4–110 kPa, and 4–7 μmol/mol, respectively. The measured spectra were fit using the sum of isolated Hartmann-Tran profiles with the addition of line mixing. For each line within the manifold, all spectroscopic parameters at room temperature were fixed to our previously obtained values (Delahaye et al., 2016, https://doi.org/10.1002/2015JD024524) and only the temperature dependences of the model parameters were adjusted. The results show that the fitted model agrees with the measured methane absorption to better than 0.3% for the entire R(6) manifold spectral region and to within 0.1% at the online position of the MERLIN for all considered pressure and temperature conditions. A first comparison with ground-based atmospheric measurement was also made showing significant improvement with respect to existing spectroscopic modeling of methane absorption.

1. Introduction

After CO_2, methane is the second most important anthropogenic greenhouse gas and is responsible for about 20% of the total radiative forcing by long-lived gases (Kirschke et al., 2013). The precise global knowledge of the CH_4 mixing ratios is required to understand the factors governing methane emissions. Existing surface measurements of methane do not have sufficient spatial coverage to adequately quantify the worldwide distribution of methane emissions. Thus, high-precision, space-borne measurement techniques are necessary to provide global coverage. Passive remote sensors such as Scanning Imaging Absorption spectroMeter for Atmospheric CHartographY (SCIAMACHY) (Frankenberg et al., 2011), Greenhouse Gases Observing Satellite (GOSAT) (Parker et al., 2011), CarbonSat (Buchwitz et al., 2013), and Sentinel 5 (Butz et al., 2012) measure the wavelength-resolved solar backscattered radiation from the surface of the Earth. However, these sensors are unable to measure at high latitudes during the winter months and their data are subject to bias in regions with aerosols layers or thin ice clouds (Morino et al., 2011). Space-borne active remote sensing is thus a complementary approach because it can be more sensitive near the surface of the Earth, essentially has zero aerosol/cloud biases and can measure during both daytime and nighttime. In order to realize this goal, Deusches Zentrum für Luft- und Raumfahrt and Centre National d'Etudes Spatiales proposed the "Methane Remote Sensing Lidar Mission" (MERLIN) in 2010 within the framework of a German-French climate-monitoring initiative (Ehret et al., 2017; Stephan et al., 2011). MERLIN is a space-borne active remote sensing instrument for retrieval of atmospheric methane (Bousquet et al., 2018; Ehret et al., 2017; Stephan et al., 2011) with an expected launch date in 2024 and a measurement principle that is based on the integrated-path differential-absorption lidar technique. The MERLIN spectrometer will measure the difference in atmospheric transmission between a laser emitting at a wavelength (online) near the center of a methane absorption feature and a reference off-line wavelength with no significant absorption (Kiemle et al., 2014, and references therein). The selected online wavelength of MERLIN is

located at the trough ($\lambda = 1.6455\ \mu m$) between two strong absorption features which belong to the R(6) manifold of the $2\nu_3$ band of $^{12}CH_4$ (Kiemle et al., 2011). By positioning the online wavelength in this absorption local minimum, the laser frequency stability requirement can be relaxed. The objective of the mission is to obtain spatial and temporal concentration gradients of atmospheric methane columns with high precision and unprecedented accuracy on a global scale. The mission targets of the measured methane column concentrations are 3.7 ppb for systematic uncertainty and a statistical uncertainty of 27 ppb for a 50-km aggregation of shot-by-shot measurements along the satellite tract (Bousquet et al., 2018). Therefore, the temperature- and pressure-dependent absorption cross sections that describe the attenuation of the radiation by methane must be known with high accuracy. Furthermore, accurate methane absorption cross sections will also improve the atmospheric spectra calculations for Earth atmospheric remote sensing in general and not only for the case of MERLIN.

In a previous study (Delahaye et al., 2016), high-quality spectra of air-broadened methane in the same $2\nu_3$ R(6) manifold region considered here were measured at room temperature with a frequency-stabilized cavity ring-down spectroscopy (FS-CRDS) system. Spectroscopic parameters of the six R(6) transitions were retrieved from these measurements using a high-order line shape model, the Hartmann-Tran (HT) profile (Ngo et al., 2013; Tennyson et al., 2014). Different pressure (i.e., intermolecular collision) effects that influence the spectral shapes such as line mixing, speed-dependent broadening and shifting and Dicke narrowing were accounted for in the analysis. It was shown that the model and fitted parameters represent the measured absorption spectra over a wide pressure range with a maximum relative residual of $\pm 0.1\%$ (Delahaye et al., 2016): the best agreement between model and experiment obtained so far for this methane manifold.

In this work, we extend the scope of our previous study by investigating the temperature dependence of the air-broadened methane absorption cross section in the MERLIN spectral region. Using the recently developed FS-CRDS spectrometer (Ghysels et al., 2017) devoted to measurements at low temperature, 27 new absorption spectra of the air-broadened methane $2\nu_3$ R(6) manifold were recorded for five temperatures, from 220 to 290 K and for various total pressures, from approximately 4 to 110 kPa. These measurements were then analyzed with the HT profile, as for the room temperature case (Delahaye et al., 2016). For each line of the manifold, all the spectroscopic parameters at room temperature were fixed to the values obtained previously (Delahaye et al., 2016) and only the temperature dependences of the first-order line mixing, as well as the pressure broadening and pressure shifting parameters were adjusted using spectra measured at 220 K. The resulting fitted model was then successfully validated by comparison with measured spectra at all other pressure and temperature conditions. A first comparison with ground-based atmospheric measurements was also made and showed significant improvement by comparison to the previous room temperature-based model.

This paper is organized as follows: Section 2 describes the experimental setup and recorded spectra, and section 3 presents the analysis procedure, the comparisons between measurements and calculations as well as the obtained spectroscopic parameters. Finally, validation of the model and associated data with ground-based measurement are described in section 4, and some conclusions are drawn in section 5.

2. Experimental Setup and Data

The measurements were based on the FS-CRDS method first described by Hodges et al. (2004) and carried out using a custom-made variable-temperature spectrometer located at the National Institute of Standards and Technology (NIST) in Gaithersburg, Maryland, USA. Extensive details about the experimental setup, which allows for measurements from 220 K to 290 K and from vacuum to atmospheric pressures, can be found in Ghysels et al. (2017). Therefore, only a brief description is given here.

The design of the ring-down cell has been studied to minimize the optical cell configuration changes related to the environment temperature variations. This characteristic allows one to perform spectroscopic measurements of metrological quality from 220 to 290 K. As reported in Ghysels et al. (2017), over the 30-min time intervals required to scan isolated carbon dioxide transitions, the temperature and frequency stabilities of the setup were better than 2 mK and within 100 kHz, respectively. However, because of the larger spectral width of the manifold investigated here, the present experiment required longer scanning times, which led to reduced cavity mode stability (nominally 1 MHz) by comparison to the low-temperature studies of Ghysels et al. (2017). Also, the main differences between the room temperature methane measurements (Delahaye et al., 2016) and the present experiment involve the superior frequency axis of the former

system where an absolute uncertainty (100-kHz level) was achieved using a Cs-clock-referenced optical frequency comb, and a long-term cavity-mode stability of 10 kHz resulted by using an active length stabilization scheme with an I_2-stabilized reference laser. In the present experiment, because an optical frequency comb was not available, the absolute frequencies were determined by a wavelength meter, which resulted in a combined uncertainty of 10 MHz.

The probe beam was provided by a distributed-feedback diode (DFB) laser followed by a booster-optical amplifier used for power amplification and rapid switching to initiate the ring-down decay events. At each spectrum step, the probe laser frequency was locked to a TEM_{00} mode of the ring-down cavity by dithering the laser frequency through a range of 1 MHz and by maximizing the rate of transmission bursts through the optical cavity as described in (Hodges & Ciuryło, 2005). With the laser frequency locked to a cavity mode, the booster-optical amplifier was switched off at constant trigger level, thereby initiating decay events of constant amplitude. At each spectrum step, 300 decays were acquired and individually fit to yield the average and standard deviation of the decay time. The line width of the incident laser beam and amount of power incident on the ring-down cavity were approximately 1 MHz and 15 mW, respectively.

Spectral scans in the forward direction (increasing frequency) and backward direction (decreasing frequency) were acquired at each temperature and pressure condition by temperature-tuning the DFB laser through successive cavity modes (separated by 187 MHz), with 130 mode jumps per 24-GHz-wide spectrum centered on the MERLIN methane absorption feature. This scanning technique involved breaking the laser lock, temperature tuning of the DFB to the next cavity mode, relocking the laser frequency, and subsequent acquisition of ring-down decays. Each jump and relock step took approximately 20 s, resulting in a minimum scan time of approximately 45 min. The baseline (empty-cavity) loss-per-unit length was nominally $\alpha_0 = 6 \times 10^{-7}$ cm^{-1} and corresponds to an intensity reflectivity of $R = 0.99995$ for the ring-down cavity mirrors. The base losses were measured at each temperature and exhibited less than 1% variation among the highest-temperature conditions but decreased by about 15% at the lowest temperature condition. The temperature-induced change in base mirror losses is attributed to movement of the optical axis of the ring-down cavity and to spatial inhomogeneities in the mirror reflectivity. Under empty-cavity conditions, the relative standard deviation and acquisition rate of the fitted decays were 0.07% and 200 Hz, respectively.

For those sample conditions corresponding to relatively high absorption losses in which $\alpha >> \alpha_0$, acquisition rates were no longer rate limited by the time for laser tuning and relocking because of the significant reduction in ring-down signal acquisition rates. At $T = 290$ K and $p = 112$ kPa, the maximum absorption losses, α, were nominally 3×10^{-6} cm^{-1} and more than 5 times greater than the base cavity losses. For this case, each scan took about 2 hr (2.5 times longer than the corresponding empty-cavity case).

The spectrum detuning axis was calculated by $\Delta\nu(q;T,p) = q\nu_F(T)/n(T,p)$ where q is an integer index, which specifies the frequency step relative to the start of the scan, $\nu_F(T)$ is the measured free spectral range of the empty cavity at T, and $n(T,p)$ is the index of refraction of the sample gas at the measurement conditions and probe laser wavelength. Details of the detuning axis calculation and uncertainty can be found in (Ghysels et al., 2017). The wavelength meter was used to locate the start of the scan relative to the MERLIN methane feature and set the absolute frequency of the initial spectrum point. To account for the finite accuracy and resolution of the wavelength meter, a small correction to this starting value was treated as a floated parameter in the fitting procedure described in section 3.

The sample pressure was monitored using a resonant Si pressure gauge with a full-scale range of 133 kPa. This pressure gauge was calibrated against a NIST secondary pressure standard, yielding a maximum relative standard uncertainty less than 0.01%. The temperature was monitored by two NIST-calibrated 100-Ω platinum resistance thermometers embedded into a hole in two of the stainless-steel flanges. The combined standard uncertainty of the temperature measurement was approximately 6 mK. For this data set, we acquired a set of spectra for five temperatures 290, 272, 257, 242, and 223 K, and various pressures, from 4 to 111 kPa. The methane-containing sample was derived from the same NIST-certified methane-in-air mixture having a molar fraction $x_{CH4} = 11.8736(33)$ μmol/mol and specified in Table 1a of Delahaye et al. (2016). At each temperature condition, the sample was introduced into the cell and backfilled with methane-free, dry air to adjust the final methane molar fraction. Samples were allowed to stabilize overnight in the cell prior to taking measurements. The molar fraction of methane in the diluted sample was estimated from the backfilling pressure ratio and the molar fraction of the certified sample. Dilution of the charge

Table 1
Summary of Experimental Conditions Indicating the Pressure P, Temperature T, and Their Relative Combined Standard Uncertainties

Spectra	P (kPa)	u(P)/P (%)	T (K)	u(T)/T (%)	x_{CH_4} (μmol/mol)
1–6	3.708–111.676	0.075–0.012	290.000	0.012	6.671
7–12	4.463–106.545	0.064–0.012	272.103	0.021	6.992
13–18	4.261–106.540	0.066–0.012	257.365	0.098	4.994
19–23	4.730–66.562	0.061–0.014	242.890	0.031	4.519
24–27	13.332–75.993	0.060–0.013	222.893	0.023	3.991

Note. The indicated molar fraction x_{CH4} of the sample gases is estimated based on the methane molar fraction of the certified source and the measured dilution ratio.

enabled optimization of the acquisition rate and signal-to-noise ratio of the spectra. A summary of experimental conditions is given in Table 1.

3. Spectra Analysis and Results

The measured spectra were analyzed using the multispectrum fitting code developed and described previously in Delahaye et al. (2016). Within this code, various line shape models can be used to represent the line profiles. The results obtained at room temperature (Delahaye et al., 2016) show that among the considered models, the HT profile (Ngo et al., 2013) combined with the first-order line mixing approximation (Rosenkranz, 1975) led to the best agreement with the measurements. The model and associated data can represent the measured spectra with a maximum relative residual of ±0.1% over a wide pressure range (Delahaye et al., 2016). Details of the functional form for the absorption coefficient can be found in Delahaye et al. (2016) and Ngo et al. (2013). Recall that in addition to the usual Doppler and the collisional broadenings, this model takes into account various refined effects. For each transition, there are five additional line shape parameters: ν_{vc}, Γ_2, Δ_2, η, and Y; ν_{vc} is the Dicke narrowing frequency, characterizing the collision-induced velocity changes effect (Nelkin & Ghatak, 1964; Rautian & Sobel'man, 1967). Γ_2 and Δ_2 represent the speed dependences of the collisional half widh and shift. The latter are modeled by the use of the quadratic speed dependence law (Rohart et al., 1994, 1997), that is, $\Gamma(v)+i\Delta(v)=\Gamma_0+i\Delta_0+(\Gamma_2+i\Delta_2)\left[(v/\tilde{v})^2-3/2\right]$, where $\tilde{v}=\sqrt{2k_BT/m}$ is the most probable speed of the absorbing molecule of mass m; η is the correlation parameter, expressing the temporal correlation between velocity changes and internal state changes. $Y=P\zeta$ is the first-order line mixing parameter and ζ the pressure-normalized line mixing coefficient, accounting for the coupling between the considered line and other lines.

The temperature dependences of the pressure broadening and shifting parameters are usually described by a power law and a linear function (see Gordon et al., 2017, and references therein), respectively. For the higher-order parameters, their temperature dependences have been investigated only in a few studies (e.g., Forthomme et al., 2015; Goldenstein & Hanson, 2015; Li et al., 2008; Wilzewski et al., 2018). These studies showed that $\Gamma_2(T)$ and $\nu_{vc}(T)$ as well as $\zeta(T)$ can be described by a similar power law as for the line broadening. For Δ_2 and η, to the best of our knowledge, there is no available experimental or theoretical information on their temperature dependences. In this work, because the sensitivity of the spectra to the temperature dependence of line shape parameters is more "tricky" than that of pressure, only the major contributions to the temperature dependence of the model were taken into account. Thus, we chose to fit only the temperature dependences of the line broadening Γ, line shifting Δ, and line mixing ζ coefficients; those of the other parameters were considered too weak to be retrieved. The considered temperature dependences were expressed as

$$\begin{aligned}\Gamma(\mathrm{v},\mathrm{T}) &= \Gamma_0\left(\frac{\mathrm{T}_0}{\mathrm{T}}\right)^{\mathrm{n}_\Gamma}+\Gamma_2\left[(\mathrm{v}/\tilde{\mathrm{v}})^2\text{-}3/2\right],\\ \mathrm{i}\Delta(\mathrm{v},\mathrm{T}) &= \mathrm{i}\left[\Delta_0+\delta'(\mathrm{T}\text{-}\mathrm{T}_0)\right]+\mathrm{i}\Delta_2\left[(\mathrm{v}/\tilde{\mathrm{v}})^2\text{-}3/2\right],\\ \zeta(\mathrm{T}) &= \zeta(\mathrm{T}_0)\left(\frac{\mathrm{T}_0}{\mathrm{T}}\right)^{\mathrm{n}_\zeta},\end{aligned} \tag{1}$$

n_Γ, δ', and n_ζ being the parameters describing the respective temperature dependences of the line broadening Γ_0, line shifting Δ_0, and line mixing ζ coefficients. Note that the speed dependence of the line

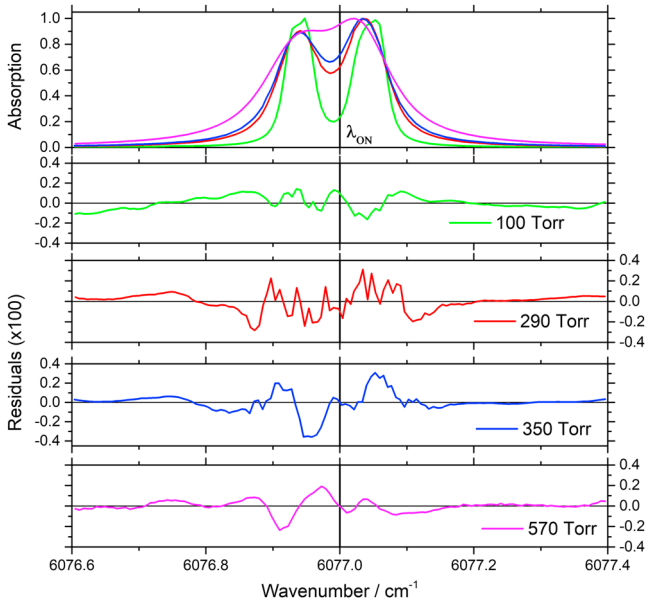

Figure 1. Peak-normalized absorption spectra (top panel) of air-broadened CH_4 in the $2\nu_3$ R(6) manifold region, measured by cavity ring-down spectroscopy at 222.893 K and various total pressures. In the lower panels are the residuals obtained from fits of the measured spectra with the HT + LM model. The Methane Remote Sensing Lidar Mission online position is indicated by the thick black line.

mixing parameter was also neglected. In the fitting procedure, the room temperature parameters of our HT + line mixing (LM) model were fixed to those obtained in Delahaye et al. (2016), and only the temperature dependences of Γ_0, Δ_0, and ζ were adjusted. To simplify the fitting procedure, in the first step, only spectra measured at the lowest temperature (i.e., 223 K, see Table 1) were considered in the fit. Furthermore, among all the recorded spectra, the spectra in this set have the highest average signal-to-noise ratio. Thus, these measured spectra should be the most sensitive to the temperature dependence of the model. Then, in the second step, the values of n_Γ, δ', and n_ζ (see equation (1)) obtained in the first step were used together with the model to compare calculated spectra with those measured at other pressure and temperature conditions. For the first step, only the parameters of the six R(6) manifold lines of $^{12}CH_4$ were adjusted during the fitting process. Recall that a multifitting procedure including spectra acquired at four pressures was used. The fits to these four spectra measured at 223 K were adjusted simultaneously, with the values of n_Γ, δ', and n_ζ for each line constrained to be the same for all pressures. For both steps of the analysis, contributions of 34 weak interfering lines were calculated using line parameters provided by the 2016 version of the HITRAN database (Gordon et al., 2017). The contribution of methane self-broadening was neglected because methane molar fractions for all measured spectra did not exceed 7 μmol/mol (see Table 1). A linear baseline with two adjustable parameters, representing the zero absorption level, and the total area for each spectrum were also retrieved. A global spectral shift for each spectrum was also adjusted because the absolute frequency of the first point of the measured frequency detuning axis was not provided with sufficient accuracy with the present setup (see section 2). The determination of the global shift for each spectrum and the temperature dependences of the line shape parameters was performed in two steps since it was impossible to fit them simultaneously. In the first step, we used the eight Fourier transform spectrometer (FTS) spectra measured at low temperature (those published in Devi et al., 2015, spectra numbers 14–21 in Table 3 of this reference) to retrieve a preliminary set of the temperature dependences of the line width, line shift, and line mixing. These FTS spectra were calibrated independently as described in Devi et al. (2015). The obtained parameters were then used to calculate spectra at the same temperature and pressure conditions as the CRDS spectra. The global shift for each CRDS spectrum was then determined through the comparison between the simulated spectrum and the CRDS measurement. In the second step, we fixed the global shift for each spectrum to the value determined previously. Then we simultaneously fit the temperature dependences of the line shape parameters using the four CRDS spectra measured at 223 K. Although some correlation between the global shift and the temperature dependences of the line shifts could remain, we believe that this correlation, if exists, is small. Furthermore, validation of our spectroscopic parameters using atmospheric spectra does not reveal any systematic residuals (See Figure 3).

The relatively long scan times at the elevated-pressure conditions made the spectra more susceptible to uncompensated drifts in the cavity length, which lead to some ambiguity in the spectrum detuning axis. See Figure 7 of Ghysels et al. (2017), in which frequency excursions (at $\lambda = 633$ nm) of cavity modes up to 5 MHz were observed over acquisition time scales spanning several hours. To quantify the effect of variation in the spectrum detuning axis, we compared forward and backward scan pairs. This analysis revealed systematic differences between the two spectra, with average peak-to-peak residual differences of 0.2% for all pairs considered. This analysis also showed that irreproducibility could be explained by variability of between 1 and 5 MHz in the cavity mode frequencies, which is consistent with the excursions measured by (Ghysels et al., 2017) on relatively long time scales.

Figure 1 shows residuals obtained from fits of the set of spectra measured at 223 K with our model as explained previously. Only the spectra obtained by scanning in the forward direction were considered. Note that all the measured spectra were normalized by their maximum absorption in the fitting procedure. For this low temperature condition, the agreement between calculated and measured spectra is on the order

Table 2
Measured Temperature Dependences of Line Parameters for the R(6) Manifold in the $2\nu_3$ Band of $^{12}CH_4$

R6 Transition	Position (cm^{-1})	n_Γ	Δ' (10^{-5} cm^{-1}/[atm K])	n_ζ
7E ← 6E 1	6,076.92716	0.672(6)	−5.81(2)	—
7F1 ← 6F2 1	6,076.93411	0.974(7)	3.39(3)	0[a]
7A1 ← 6A2 1	6,076.95316	0.662(2)	−0.69(3)	2.73(51)
7F1 ← 6F2 2	6,077.02785	0.783(5)	−3.76(2)	0.87(62)
7F2 ← 6F1 1	6,077.04639	0.845(4)	3.06(4)	2.28(76)
7A2 ← 6A1 1	6,077.06296	0.682(2)	1.92(5)	4.54(62)

Note. The uncertainties in parentheses are 1σ internal statistical errors in the last quoted digit(s). Values can be converted to SI units using the factor 1 cm^{-1} atm^{-1} = 0.295872 MHz/Pa.
[a]Ill-defined parameter, set to 0.

of ±0.3% of the peak absorption and better near the MERLIN online region (i.e., less than ±0.1% at 1.64555 μm). Again, we see evidence that some measured spectra, especially at low pressure, are affected by uncertainty in the spectrum detuning axis discussed above which we attribute to small frequency drift (linked to temperature variations) of the cavity mode positions over the scan time. For the reasons discussed above, the present result is not as good as what was obtained with a room temperature spectrometer where fit residuals better than ±0.1% were demonstrated (Delahaye et al., 2016). However, with experimental challenges and difficulty in accurately modeling strongly overlapped lines at such low temperature, the present study constitutes the best result obtained so far for a methane manifold. Note that neglecting the temperature dependences of Γ, Δ, and ζ in the spectra calculations at low temperature leads to large errors, with spectral residuals that can be as much as 10% at 223 K, for instance.

The retrieved temperature dependences of the line parameters for the $2\nu_3$ R(6) $^{12}CH_4$ manifold are listed in Table 2 together with their associated standard deviations (1σ statistical errors reported by the fitting program). We believe that our set of parameters for the temperature dependence together with our room temperature model provide the best available model to date for the absorption in the R(6) manifold of the $2\nu_3$ band of $^{12}CH_4$ over large pressure and temperature ranges. The obtained parameters are in a range of "physical" values, with the notable exception of the temperature dependence of the line mixing parameters n_ζ as it was also the case with line mixing ζ values of the room temperature model (Delahaye et al., 2016). In fact, because of the strong overlap between the considered R(6) transitions, the first-order approximation does not adequately describe the line mixing effect. This leads to effective line mixing parameters that do not satisfy the sum rule and to some large values of the temperature dependence parameters (see Table 2). Note that we chose to use the first-order line mixing approximation instead of the full relaxation matrix as done in Tran et al. (2010) and Devi et al. (2015) since the latter would involve a larger number of parameters to be retrieved. Furthermore, the use of the full relaxation matrix together with the HT profile would be too time consuming, making this approach incompatible with atmospheric applications. Since first-order line mixing parameters were obtained here for large ranges of pressure and temperature (see Table 1), they are fully applicable within these temperature and pressures ranges, which are sufficient for most atmospheric applications.

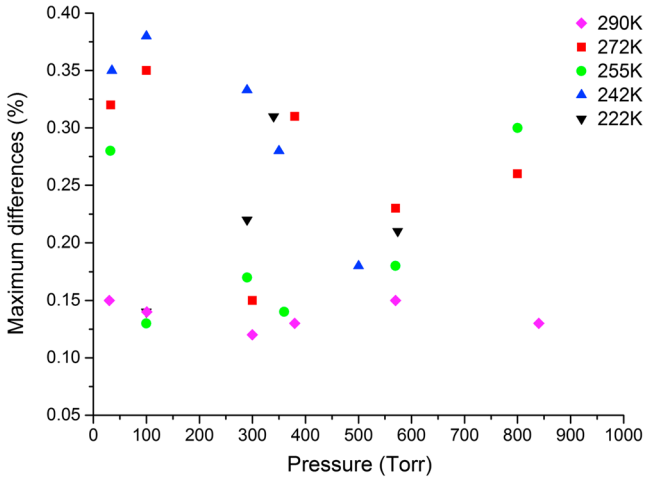

Figure 2. Maximum residuals (%) for all considered pressure and temperature conditions.

The obtained parameters and model were then used to calculate various spectra at the same pressure, temperature, and gas concentration conditions as those of the measurements for the other temperatures (see Table 1). The simulated spectra then were directly compared with the measurements, with only a global frequency shift, a linear baseline and the total area being adjusted for each case. Because it would have been unreadable to present a graph by spectrum or temperature, we chose to evaluate the (absolute) maximum difference between the measurement and calculation for each spectrum and to summarize the results in a single graph. Figure 2 shows these maximum deviations between observed and calculated spectra obtained for all considered pressure and temperature

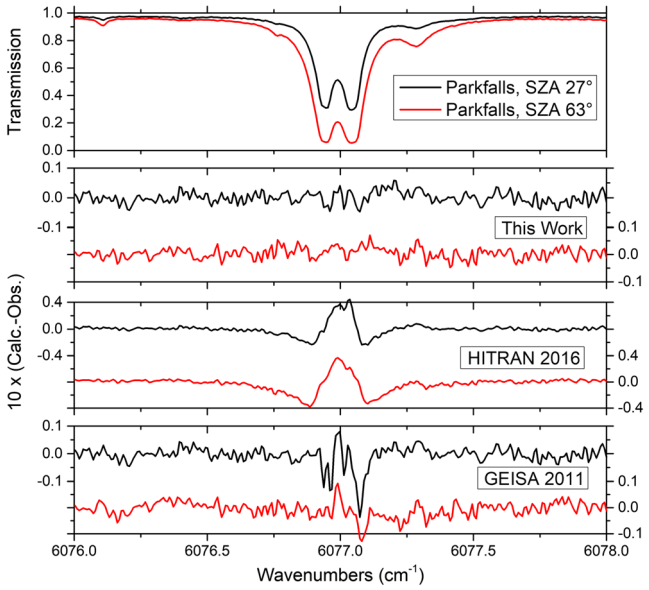

Figure 3. (top) Ground-based transmission spectra measured by Fourier transform spectrometer at Park Falls for two solar zenith angles (SZAs; top panel) in the CH_4 $2\nu_3$ R(6) manifold spectral region. Residuals obtained from fits of these measurements using methane spectroscopic data and model of the present work are plotted in the second panel, while those obtained from the 2016 version of HITRAN (Gordon et al., 2017) and GEISA2009 (Jacquinet-Husson et al., 2011) are shown in the third and fourth panels, respectively.

conditions (see Table 1). First of all, the results obtained near room temperature (290 K) are in excellent agreement with our previous observations using our room temperature model (Delahaye et al., 2016), with a maximum deviation of about ±0.1%. Second, the low pressure spectra are generally more sensitive to uncertainties in the frequency axis, which explains the relatively higher discrepancies observed for pressures below about 50 kPa. However, accounting for all pressure and temperature conditions presented in Table 1, the maximum deviations observed are of the order of ±0.3%. Given the large pressure and temperature ranges, and the effect associated with uncertainty in the spectrum frequency detuning axes, we consider this result to be quite satisfactory.

4. Comparison With Ground-Based Atmospheric Measurements

The resulting spectroscopic model and coefficients were then validated by comparison with atmospheric measurements. Two ground-based solar absorption spectra, measured at two different solar zenith angles, 27° and 68°, were chosen for this test. These spectra were recorded at the Total Carbon Column Observing Network (TCCON; Wunch et al., 2011) facility in Park Falls, Wisconsin, on 3 July and 10 August 2008, respectively. Only the 6,076- to 6,078-cm^{-1} spectral range region was considered in the comparison. Calculations were made using the Spectroscopic Parameters And Radiative Transfer Evaluation calibration/validation chain developed in our group and widely described in Armante et al. (2016). The temperature and pressure profiles used in our calculations were taken from the National Centers for Environmental Prediction database, atmospheres being divided into 71 layers with a layer height of 1 km. The temperature, pressure, and gas volume mixing ratio were linearly interpolated within each layer. Absorption features by CH_4, H_2O, and CO_2 were accounted for in the calculation. Typical standard summer profiles coming from climatological models, shifted to adjust the total column amount of gas to that given by TCCON, were used as a priori profiles. Contributions of CO_2, H_2O, and weak methane lines were calculated using spectroscopic data provided by the latest version of the HITRAN database (Gordon et al., 2017). For the six intense lines of the $2\nu_3$ R(6) manifold, three calculations were performed: In the first case, the present spectroscopic data and model were used, whereas in the second and third cases, we used data from the HITRAN 2016 (Gordon et al., 2017) and GEISA 2009 (Jacquinet-Husson et al., 2011) databases, respectively. Note that in the two last cases, the Voigt profile was used to model the absorption lines. The calculated spectra, convolved with the apparatus line shape function provided by the TCCON station were then fitted to the measurements. In the fitting procedure, a scaling factor applied to the a priori profiles was retrieved for each molecular species. A linear baseline was also adjusted for each considered spectrum.

Figure 3 shows the comparisons between the calculated and measured TCCON spectra. As can be observed, the present spectroscopic data and model lead to the best agreement with the measurements, with the residuals being completely within the experimental noise. This result therefore fully confirms the quality of our measurements and spectrum modeling. Conversely, we find large discrepancies between the measured spectra and the spectra calculated using HITRAN 2016 and GEISA 2009 parameters. The spectroscopic data in GEISA 2009 came from Frankenberg et al. (2008) in which the line mixing effect was taken into account through ad hoc line broadening and shifting coefficients, whereas line mixing is completely neglected in the data of HITRAN 2016. This difference between the two models explains why the GEISA 2009 results are better than those obtained using HITRAN 2016.

These results show that our new model results in significant improvement in the atmospheric spectra calculations. The retrieved values of the scaling factor applied to the initial profile of CH_4, obtained with our spectroscopic parameters, and those of GEISA 2009 and HITRAN 2016 are respectively 1.005, 0.990, and 0.950 for the spectrum measured at 68° and 0.999, 0.981, and 0.998 for that measured at 27°. These results show that

the three sets of spectroscopic data lead to large differences in the retrieved methane quantity. Further investigations of atmospheric observations for various air masses and in which the retrieved methane volume mixing ratio is validated with reference measurements will be performed in a future study.

5. Conclusions

Precise modeling of methane absorption cross section in the 1.64-μm region for atmospheric temperature and pressure conditions is needed to meet the accuracy requirement of the MERLIN. In a previous study (Delahaye et al., 2016), using high-quality laboratory measurements and the most advance line shape model, we deduced a set of room temperature spectroscopic data capable of representing the measured cross sections over a wide pressure range with a maximum relative residual of ±0.1%. In this work, we investigated the temperature dependences of methane absorption cross section in the MERLIN spectral region. To this aim, the absorption of methane in the 1.64-μm region was measured using an FS-CRDS system for various temperature and pressure conditions. The measured spectra were analyzed using the same profile as for the case of room temperature study (which accounts for line mixing, Dicke narrowing, and speed dependence effects). The resulting fit coefficients and model enable calculation of synthetic spectra to within 0.3% of measurements and yield even better agreement at the online position of the MERLIN (differences of less than 0.1%). Comparisons between the new model and ground-based atmospheric measurement were made and show significant improvement with respect to existing spectroscopic models of methane absorption in this spectral region. The results from this work can be readily applied not only to the MERLIN but also for Earth atmospheric remote sensing in general (e.g., TCCON, Greenhouse Gases Observing Satellite, and Network for the Detection of Atmospheric Composition Change).

Acknowledgments
The authors thank J. -M. Hartmann for helpful discussions and Manfred Birk for investigating the irregularities in the spectrum detuning axis. T. Delahaye, R. Armante, and H. Tran were supported by the French Space Agency, Centre National d'Etudes Spatiales, whereas M. Ghysels and J. T. Hodges were supported by the NIST Greenhouse Gas Measurement and Climate Research Program. Part of the research described in this article was performed at the Jet Propulsion Laboratory, California Institute of Technology, under contracts and cooperative agreements with the National Aeronautics and Space Administration. The measured spectra are available on https://osf.io/6YSGV.

References

Armante, R., Scott, N., Crevoisier, C., Capelle, V., Crepeau, L., Jacquinet, N., & Chédin, A. (2016). Evaluation of spectroscopic databases through radiative transfer simulations compared to observations. Application to the validation of GEISA 2015 with IASI and TCCON. *Journal of Molecular Spectroscopy*, *327*, 180–192. https://doi.org/10.1016/j.jms.2016.04.004

Bousquet, P., Pierangelo, C., Bacour, C., Marshall, J., Peylin, P., Ayar, P. A., et al. (2018). Error budget of the Methane Remote LIdar missioN and its impact on the uncertainties of the global methane budget. *Journal of Geophysical Research: Atmospheres*, *123*, 11,766–11,785. https://doi.org/10.1029/2018JD028907

Buchwitz, M., Reuter, M., Bovensmann, H., Pillai, D., Heymann, J., Schneising, O., et al. (2013). Carbon monitoring satellite (CarbonSat): Assessment of atmospheric CO_2 and CH_4 retrieval errors by error parameterization. *Atmospheric Measurement Techniques*, *6*(12), 3477–3500. https://doi.org/10.5194/amt-6-3477-2013

Butz, A., Galli, A., Hasekamp, O., Landgraf, J., Tol, P., & Aben, I. (2012). TROPOMI aboard Sentinel-5 Precursor: Prospective performance of CH_4 retrievals for aerosol and cirrus loaded atmospheres. *Remote Sensing of Environment*, *120*, 267–276. https://doi.org/10.1016/j.rse.2011.05.030

Delahaye, T., Maxwell, S. E., Reed, Z. D., Lin, H., Hodges, J. T., Sung, K., et al. (2016). Precise methane absorption measurements in the 1.64μm spectral region for the 442 MERLIN mission. *Journal of Geophysical Research: Atmospheres*, *121*, 7360–7370. https://doi.org/10.1002/2016JD025024

Devi, V. M., Benner, D. C., Sung, K., Crawford, T. J., Yu, S., Brown, L. R., et al. (2015). Self- and air-broadened line shapes in the $2\nu_3$ P and R branches of $^{12}CH_4$. *Journal of Molecular Spectroscopy*, *315*, 114–136. https://doi.org/10.1016/j.jms.2015.05.003

Ehret, G., Bousquet, P., Pierangelo, C., Alpers, M., Millet, B., Abshire, J., et al. (2017). MERLIN: A French-German space lidar mission dedicated to atmospheric methane. *Remote Sensing*, *9*(10), 1052. https://doi.org/10.3390/rs9101052

Farges, T., & Blanc, E. (2016). Characteristics of lightning, sprites, and human-induced emissions observed by nadir-viewing cameras on board the International Space Station. *Journal of Geophysical Research: Atmospheres*, *121*, 3405–3420. https://doi.org/10.1002/2015JD024524

Forthomme, D., Cich, M. J., Twagirayezu, S., Hall, G. E., & Sears, T. J. (2015). Application of the Hartmann–Tran profile to precise experimental data sets of $^{12}C_2H_2$. *Journal of Quantitative Spectroscopy and Radiative Transfer*, *165*, 28–37. https://doi.org/10.1016/j.jqsrt.2015.06.013

Frankenberg, C., Aben, I., Bergamaschi, P., Dlugokenckv, E. J., van Hees, R., Houweling, S., et al. (2011). Global column averaged methane mixing ratios from 2003 to 2009 as derived from SCIAMACHY: Trends and variability. *Journal of Geophysical Research*, *116*, D04302. https://doi.org/10.1029/2010JD014849

Frankenberg, C., Warneke, T., Butz, A., Aben, I., Hase, F., Spietz, P., & Brown, L. R. (2008). Pressure broadening in the $2\nu_3$ band of methane and its implication on atmospheric retrievals. *Atmospheric Chemistry and Physics*, *8*(3), 10,021–10,055. https://doi.org/10.5194/acpd-8-10021-2008

Ghysels, M., Liu, Q., Fleisher, A. J., & Hodges, J. T. (2017). A variable-temperature cavity ring-down spectrometer with application to line shape analysis of CO_2 spectra in the 1600 nm region. *Applied Physics B*, *123*(4), 1–13. https://doi.org/10.1007/s00340-017-6686-y

Goldenstein, C. S., & Hanson, R. K. (2015). Diode-laser measurements of linestrength and temperature-dependent lineshape parameters for H2O transitions near 1.4μm using Voigt, Rautian, Galatry, and speed-dependent Voigt profiles. *Journal of Quantitative Spectroscopy and Radiative Transfer*, *152*, 127–139. https://doi.org/10.1016/j.jqsrt.2014.11.008

Gordon, I., Rothman, L. S., Hill, C., Kochanov, R. V., Tan, Y., Bernath, P. F., et al. (2017). The HITRAN2016 molecular specoscopic database. *Journal of Quantitative Spectroscopy and Radiative Transfer*, *130*, 4–50. https://doi.org/10.1016/j.jqsrt.2013.07.002

Hodges, J. T., & Ciuryło, R. (2005). Automated high-resolution frequency-stabilized cavity ring-down absorption spectrometer. *Review of Scientific Instruments*, *76*(2), 023112. https://doi.org/10.1063/1.1850633

Hodges, J. T., Layer, H. P., Miller, W. W., & Scace, G. E. (2004). Frequency-stabilized single-mode cavity ring-down apparatus for high-resolution absorption spectroscopy. *Review of Scientific Instruments*, *75*(4), 849–863. https://doi.org/10.1063/1.1666984

Jacquinet-Husson, N., Armante, R., Scott, N. A., Chédin, A., Crépeau, L., Boutammine, C., et al. (2011). The 2009 edition of the GEISA spectroscopic database. *Journal of Molecular Spectroscopy*, *327*, 31–72. https://doi.org/10.1016/j.jms.2016.06.007

Kiemle, C., Kawa, S. R., Quatrevalet, M., & Browell, E. V. (2014). Performance simulations for a spaceborne methane lidar mission. *Journal of Geophysical Research: Atmospheres*, *119*, 3600–3614. https://doi.org/10.1002/2013JD021290

Kiemle, C., Quatrevalet, M., Ehret, G., Amediek, A., Fix, A., & Wirth, M. (2011). Sensitivity studies for a space-based methane lidar mission. *Atmospheric Measurement Techniques*, *4*(10), 2195–2211. https://doi.org/10.5194/amt-4-2195-2011

Kirschke, S., Bousquet, P., Ciais, P., Saunois, M., Canadell, J. G., Dlugokencky, E. J., et al. (2013). Three decades of global methane sources and sinks. *Nature Geoscience*, *6*(10), 813–823. https://doi.org/10.1038/ngeo1955

Li, H., Farooq, A., Jeffries, J. B., & Hanson, R. K. (2008). Diode laser measurements of temperature-dependent collisional-narrowing and broadening parameters of Ar-perturbed H2O transitions at 1391.7 and 1397.8nm. *Journal of Quantitative Spectroscopy and Radiative Transfer*, *109*(1), 132–143. https://doi.org/10.1016/j.jqsrt.2007.05.008

Morino, I., Uchino, O., Inoue, M., Yoshida, Y., Yokota, T., Wennberg, P. O., et al. (2011). Preliminary validation of column-averaged volumemixing ratio of carbon dioxide and methane retrieved from GOSAT short-wavelength infrared spectra. *Atmospheric Measurement Techniques*, *4*(6), 1061–1076. https://doi.org/10.5194/amt-4-1061-2011

Nelkin, M., & Ghatak, A. (1964). Simple Binary Collision Model for Van Hove'sGs(r, t). *Physical Review*, *135*(1A), A4–A9. https://doi.org/10.1103/PhysRev.135.A4

Ngo, N. H., Lisak, D., Tran, H., & Hartmann, J. M. (2013). An isolated line-shape model to go beyond the Voigt profile in spectroscopic databases and radiative transfer codes. *Journal of Quantitative Spectroscopy and Radiative Transfer*, *129*, 89–100. https://doi.org/10.1016/j.jqsrt.2013.05.034

Parker, R., Boesch, H., Cogan, A., Fraser, A., Feng, L., Palmer, P. I., et al. (2011). Methane observations from the greenhouse gases observing SATellite: Comparison to ground based TCCON data and model calculations. *Geophysical Research Letters*, *38*, L15807. https://doi.org/10.1029/2011GL047871

Rautian, S. G., & Sobel'man, I. I. (1967). The effect of collisions on the Doppler broadening of spectral lines. *Soviet Physics Uspekhi*, *9*(5), 701–716. https://doi.org/10.1070/PU1967v009n05ABEH003212

Rohart, F., Ellendt, A., Kaghat, F., & Mader, H. (1997). Self and polar foreign gas line broadening and frequency shifting of CH3F: Effect of the speed dependence observed by millimeter-wave coherent transients. *Journal of Molecular Spectroscopy*, *185*(2), 222–233. https://doi.org/10.1006/jmsp.1997.7395

Rohart, F., Mader, H., & Nicolaisen, H.-W. (1994). Speed dependence of rotational relaxation induced by foreign gas collisions: Studies on CH3F by millimeter wave coherent transients. *The Journal of Chemical Physics*, *101*(8), 6475–6486. https://doi.org/10.1063/1.468342

Rosenkranz, P. (1975). Shape of the 5 mm oxygen band in the atmosphere. *IEEE Transactions on Antennas and Propagation*, *23*(4), 498–506. https://doi.org/10.1109/TAP.1975.1141119

Stephan, C., Alpers, M., Millet, B., Ehret, G., Flamant, P., & Daniel, C. (2011). MERLIN: A space-based methane monitor. In *Proc. SPIE 8159,* Lidar Remote Sensing for Environmental Monitoring XII.

Tennyson, J., Bernath, P. F., Campargue, A., Császár, A. G., Daumont, L., Gamache, R. R., et al. (2014). Recommended isolated-line profile for representing high-resolution spectroscopic transitions (IUPAC technical report). *Pure and Applied Chemistry*, *86*(12), 1931–1943. https://doi.org/10.1515/pac-2014-0208

Tran, H., Hartmann, J.-M., Toon, G., Brown, L. R., Frankenberg, C., Warneke, T., et al. (2010). The $2\nu_3$ band of CH_4 revisited with line mixing: Consequences for spectroscopy and atmospheric retrievals at 1.67μm. *Journal of Quantitative Spectroscopy and Radiative Transfer*, *111*(10), 1344–1356. https://doi.org/10.1016/j.jqsrt.2010.02.015

Wilzewski, J. S., Birk, M., Loos, J., & Wagner, G. (2018). Temperature-dependence laws of absorption line shape parameters of the CO2 ν3band. *Journal of Quantitative Spectroscopy and Radiative Transfer*, *206*, 296–305. https://doi.org/10.1016/j.jqsrt.2017.11.021

Wunch, D., Toon, G. C., Blavier, J. F. L., Washenfelder, R. A., Notholt, J., Connor, B. J., et al. (2011). The total carbon column observing network. *Philosophical Transactions of the Royal Society A: Mathematical, Physical and Engineering Sciences*, *369*(1943), 2087–2112. https://doi.org/10.1098/rsta.2010.0240